An Agent-Based Model of Monocyte Differentiation into Tumour-Associated Macrophages in Chronic Lymphocytic Leukemia

Nina Verstraete[a,b], Malvina Marku[a,b], Marcin Domagala[a,b], Hélène Arduin[a,b], Julie Bordenave[a,b], Jean-Jacques Fournié[a,b], Loïc Ysebaert[a,b,d], Mary Poupot[a,b], and Vera Pancaldi[a,b,c]

[a]INSERM, Cancer Research Center of Toulouse, 2 Avenue Hubert Curien, 31037, CEDEX 1 Toulouse, France; [b]Université Toulouse-III Paul Sabatier, Route de Narbonne, 31330 Toulouse, France; [c]Barcelona Supercomputing Center, Carrer de Jordi Girona, 29, 31, 08034 Barcelona, Spain; [d]Service d'Hématologie, Institut Universitaire du Cancer de Toulouse-Oncopole, 31330 Toulouse, France

Monocyte-derived macrophages are immune cells which help maintain tissue homeostasis and defend organisms against pathogens. In solid tumors, recent studies have uncovered complex macrophage populations, among which tumor-associated macrophages, supporting tumorigenesis through multiple cancer hallmarks such as immunosuppression, angiogenesis or matrix remodeling. In the case of chronic lymphocytic leukemia, these macrophages are known as nurse-like cells and have been shown to protect leukemic cells from spontaneous apoptosis and contribute to their chemoresistance. We propose an agent-based model of monocytes differentiation into nurse-like cells upon contact with leukemic B cells *in-vitro*. We studied monocyte differentiation and cancer cells survival dynamics depending on diverse hypotheses on monocytes and cancer cells relative proportions, sensitivity to their surrounding environment and cell-cell interactions. Peripheral blood mononuclear cells from patients were cultured and monitored during 13 days to calibrate the model parameters, such as phagocytosis efficiency, death rates or protective effects from the nurse-like cells. Our model is able to reproduce experimental results and predict cancer cells survival dynamics in a patient-specific manner. Our results shed light on important factors at play in cancer cells

survival, such as macrophage and nurse-like cell phagocytosis efficiencies or cell sensing distances.

Introduction

Advances in cancer therapies involving a better understanding of the role of immune cells inside tumors have led to a dramatic improvement in patient response to therapies and survival. These therapies are based on the reactivation of immune cells that normally detect and eliminate cancer cells and whose cytotoxic activity is inhibited within tumors. However, the great progress offered by these approaches is hampered by the ineffectiveness of these therapies in around two thirds of the patients (1) through either primary or acquired resistance, associated to relapse in initially responding patients. Additionally, these immunotherapies can present a series of strong side effects ranging from rare deadly conditions to highly uncomfortable autoimmune chronic conditions affecting some of the patients considered 'cured' from their cancers. The revolution of immune therapies resulted in a paradigm shift in our understanding of cancer and the more we discover about the various cells present in tumors and the specific ways in which they interact with each other, the better we will be able to tune the tumor microenvironment (TME) to arrest tumor growth.

In recent years, the research focus has been mostly on anti-tumoral T lymphocytes but in many cancers the presence of myeloid cells interferes with their killing action. In this project, we aim to better characterize the myeloid cells which protect the cancer cells from attack by T cells promoting tumor growth. It has long been known that tumors involve high levels of inflammation and for this reason macrophages are found in abundance in tumor biopsies. Macrophages can be either derived from monocytes in the blood or found in the tumor and are usually described to be in two opposite states as pro-inflammatory (M1) or anti-inflammatory (M2) macrophages, depending on their environmental signals (2, 3). However, recent single cell studies identified a broader spectrum of phenotypes also impacting their specific functions such as phagocytosis, immunoregulation, matrix deposition, tissue remodeling and tumor resistance (4). In tumors, macrophages can be educated by the cancer cells to promote their growth, becoming Tumor Associated Macrophages (TAMs) (5, 6). Activation of the TAMs polarization pathway leads to the secretion of several cytokines, such as CXCL12/13, IL-10, and IL-6/IL-8, which are reported to have pro-tumoral effect (7, 8), providing protection to the cancer cells.

A similar ecology of cancer cells and macrophages is established in the case of Chronic Lymphocytic Leukemia (CLL), a blood borne malignancy characterized by the accumulation of large quantities of $CD19^+/CD5^+$ B cancer cells. These cells can be encountered in the bloodstream but also in lymphoid organs (bone-marrow, spleen and lymph nodes) forming proliferating centers in which these cells accumulate at high densities, promoting disease progression (9–12). B-CLL are unable to proliferate on their own and need to migrate to proliferation centers where they encounter a supportive TME comprising T cells, stromal cells and TAMs, which are called Nurse-like cells (NLCs) in this pathology. It has been widely reported that NLCs are crucial in rescuing B-CLL from spontaneous apoptosis and are important in attracting them to the proliferation centers (13).

Similarly to cancer cells in solid tumors, B-CLL cells are able to induce the differentiation of monocytes into NLCs through direct contact and cytokine production, which will favor the establishment of a pro-tumoral environment, protecting the leukaemic cells from spontaneous apoptosis, often leading to therapy resistance (14). One of the limitations in the study of TAMs is the difficulty in identifying them in bulk tumor samples, due to their close similarity with other macrophages that are also present in the TME. However, we showed that although NLCs and M2-type macrophages display a similar profile in the CLL microenvironment (15), some distinctions can be highlighted, such as high expression of the RAGE membrane receptor, the HIF1α and VEGF/EGF transcription factors in NLCs (16). Given the nurturing properties of NLCs in the CLL microenvironment, a high number of NLCs has been reported to lead to disease progression and shorter overall survival (17, 18). It has also been reported that NLCs express high levels of stromal-derived factor 1-α (SDF-1α), a potent chemoattractant for CLL cells inducing their migration and emperipolesis, the presence of entire CLL cells inside macrophages (19). Beside release of soluble factors, NLCs can also rescue B-CLL by direct contact (20). Other molecules released by NLCs such as BAFF, BDNF and APRIL have been reported to support survival of B-CLL (21, 22). However, the detailed mechanisms that lead to the formation of NLCs remain to be fully elucidated. Importantly, the formation of NLCs can be observed and studied with a biologically relevant *in-vitro* system in which patient-derived Peripheral Blood Mononuclear Cells (PBMCs) are cultured for a few days. PBMCs are usually composed of 1-3% monocytes and >95% B-CLL cells, depending on the patient and stage disease. Heterologous *in-vitro* co-cultures of healthy monocytes and patient-derived B-CLL cells can also be used to

produce NLCs in the absence of any other cell type. These two systems constitute a great resource to dissect the detailed processes that take place during the differentiation of monocytes into macrophages and their polarization into NLCs. Moreover, controllable settings in this experiment allow a detailed investigation of the conditions that are necessary and sufficient for NLCs production and make it a perfect tool to develop computational models of this process.

Agent-based models (ABMs) represent a discrete modeling approach that enables the simulation of the dynamics of populations of individuals in an environment. In principle, ABMs consist of decentralized agents which can be grouped into classes defined by their own characteristics and behavioral rules in space and time. This structure enables us to study the global behavior and the emergent properties of the system produced at the population level (23, 24). Importantly, contrary to other equation-based models (25–27), the deterministic or stochastic dynamics is spatio-temporal, enabling the identification of spatial patterns of individuals in time. In cancer biology, ABMs have been widely used to simulate the dynamics of diverse immune and cancer cells populations (25, 28–30). Specifically, models have investigated properties of tumor morphology, adaptation of cancer cells in the TME, mutations and phenotype diversity, cell plasticity, the role of the extracellular matrix, and the effect of drugs and nutrition on tumor survival and proliferation (31–36). Over the years, a number of computational tools for implementing ABMs have been developed, including advanced methods for incorporating both inter- and intra-cellular interactions to simulate the global dynamics of multicellular systems (37, 38). Here, we present an ABM implemented in Netlogo (39, 40) aiming to reproduce monocyte differentiation into macrophages and polarization into NLCs upon contact with B-CLL cells. We calibrate it on *in-vitro* cultures of CLL patient PBMCs and perform extensive parameter optimization using parameter exploration based on genetic algorithms integrated in the OpenMOLE framework (41). The model allows us to gain quantitative insights into important factors and cellular processes in this biological system, such as phagocytosis and anti-apoptotic signaling mechanisms that protect CLL cells from apoptosis.

Results

NLC formation *in-vitro*. In order to observe the formation of NLCs *in-vitro*, autologous cultures from three CLL patients PBMCs were monitored during 13 days (Fig. 1A). Daily observation allowed us to see outgrowth of big, adherent NLCs, whose phenotype was further assessed by flow cytometry (see Methods,

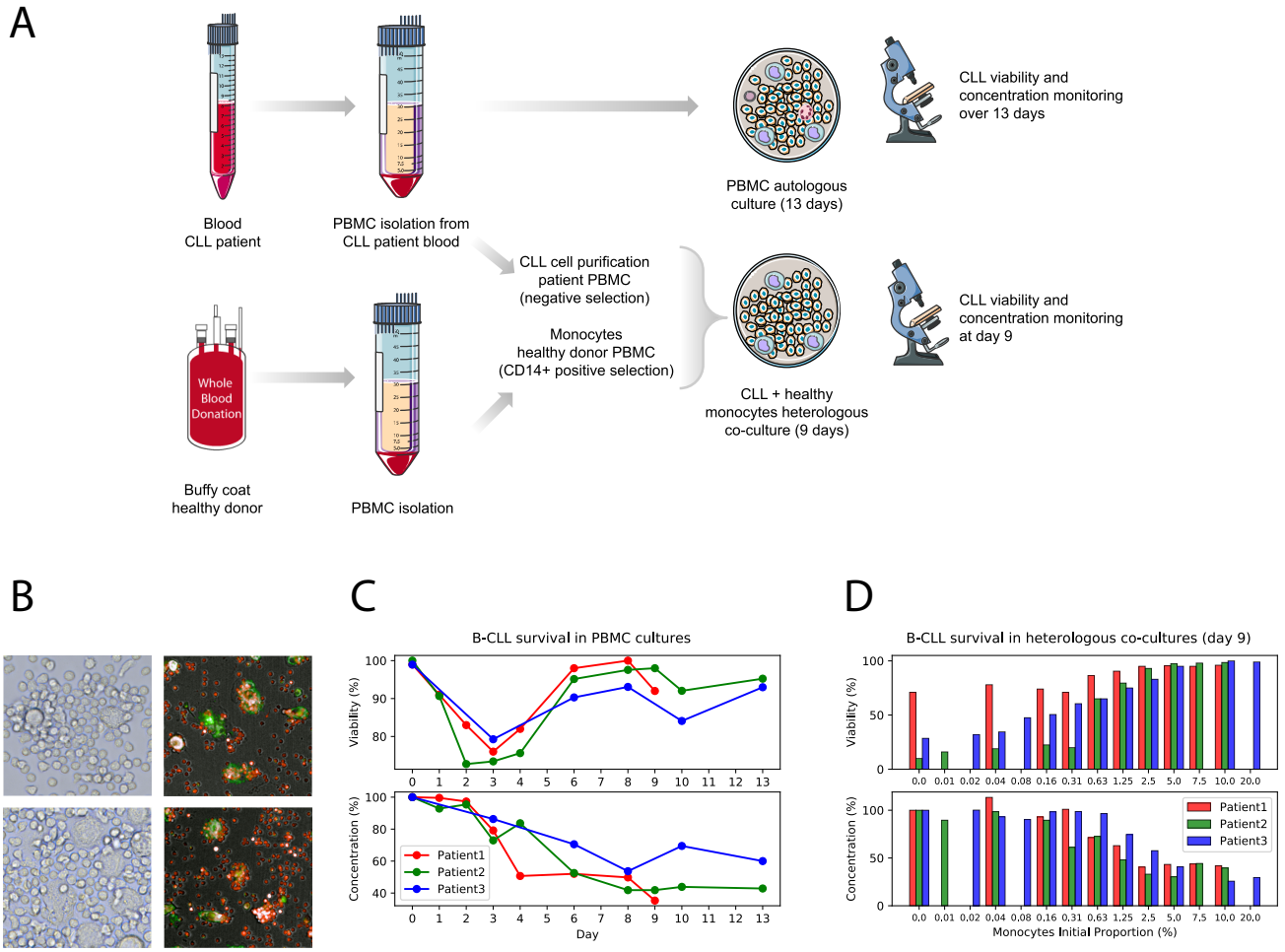

Fig. 1. Experimental setups and datasets from *in-vitro* PBMC cultures from CLL patients. A) Experimental set-up. Autologous and heterologous co-cultures of B-CLL and monocytes leading to NLC production. In autologous cultures, Peripheral Blood Mononuclear Cells (PBMC) were isolated from CLL patients' blood samples and cultured *in-vitro* for 13 days. The cell concentration and viability of B-CLL was monitored at indicated time points by haemocytometer and flow cytometry AnnexinV/7AAD staining respectively. **B) Visualization of NLCs at 10 days of *in-vitro* culture from two different patients** in bright-field and immunofluorescence microscopy (NLCs: green staining; B-CLL: red staining). **C) Time course datasets produced from the PBMC autologous cultures.** B-CLL cells survival was monitored by viability assay and concentration measurements. **D) Heterologous co-cultures.** Monocytes from healthy donors and B-CLL were co-cultured to assess the relationship between the initial density of monocytes and the level or survival of B-CLL after 9 days. The x-axis displays different monocytes initial proportions (not to scale for clarity). Measurements resulting from duplicates on the same patient were averaged. The complete data showing patient intra variability is available in Supplementary Material.

Cell culture for the complete experimental protocol applied). An example of visualization of NLCs (green staining) by immunofluorescence microscopy is shown in Fig. 1B. Additionally, concentration and viability of B-CLL were measured at the indicated time points (Fig. 1C). Based on the changes in morphology and expression of myeloid markers of maturating NLCs (CD11c, CD14, CD16, CD163 and CD206) and on the state of B-CLL cells, we have distinguished 4 stages of the culture which allowed us to specify global and local behaviors in the ABM design:

- **Day0 - Day3**. The initial state of the culture is characterized by the presence of approximately 6% of apoptotic B-CLL cells as a result of post-isolation stress and the initial lack of pro-survival agents. Monocytes attach to the plastic of the culture dish and start differentiation into macrophages. Based on the B-CLL cell countings, the phagocytosis activity of the differentiating monocytes is low, resulting in a decrease in the overall B-CLL viability. The distinction between M1 or M2 is not depicted in detail, but a killing efficiency activity from the Macrophage class is explored (0% to 5% probability that a macrophage phagocytes a living B-CLL cell).

- **Day3 - Day6**. Maturation of macrophages/NLCs continues and phagocytosis of the dead and apoptotic B-CLL cells intensifies, this phenomenon is called efferocytosis. The global B-CLL viability increases and concentration decreases.

- **Day6 - Day10**. Macrophages/NLCs reach maturation. We observe a tendency for B-CLL cells to accumulate around NLCs. B-CLL cell viability and concentration starts stabilizing.

- **Day10 - Day13**. The culture enters the steady state phase. B-CLL viability remains around 95% and cell concentration remains constant reaching 40-50% of the initial concentration.

An agent-based model of NLCs formation. The B-CLL survival dynamics observed *in-vitro* can be described as the evolution of a system composed by two main cell populations (Fig. 2A) : cancer cells (B-CLL) and myeloid cells (monocytes, macrophages, NLCs). Cancer cells can be found in 3 states, depending on their life status: (i) need-signal (red arrow), when they are still above the apoptosis threshold and are attracted by chemotaxis to anti-apoptotic signals from NLCs, (ii) apoptotic (yellow arrow), an irreversible state in which the cells will continue to move and eventually die and (iii) dead (grey arrow), when the cells have reached the death threshold and will remain immobile. Myeloid cells can be found under 3 states as well,

corresponding to their differentiation and polarization state: (i) monocyte, (ii) macrophage or (iii) NLC, characterized by specific properties and spatio-temporal behaviors in terms of different actions including movement, phagocytosis (efferocytosis) or cell-cell interactions (Fig. 2B). From the dynamics shown in Fig. 1C, microscopy observations and flow cytometry data on the evolution of the NLC phenotype (data not shown), we deduced global behaviors that might be at play in the cells' interactions (see Methods section for a detailed description of the rules). The model also has a series of parameters that could either be calibrated based on experimental observations or optimized through a parameter exploration that minimizes the difference between the predicted B-CLL cell viability and concentration and the corresponding experimental data from autologous PBMC culture throughout the 13 days shown in (Fig. 1C). Parameter optimization was performed on simulations with 1000 cells, including 1.6% monocytes (experimental estimation averaged from 3 patients), and a total cell density of 55%.

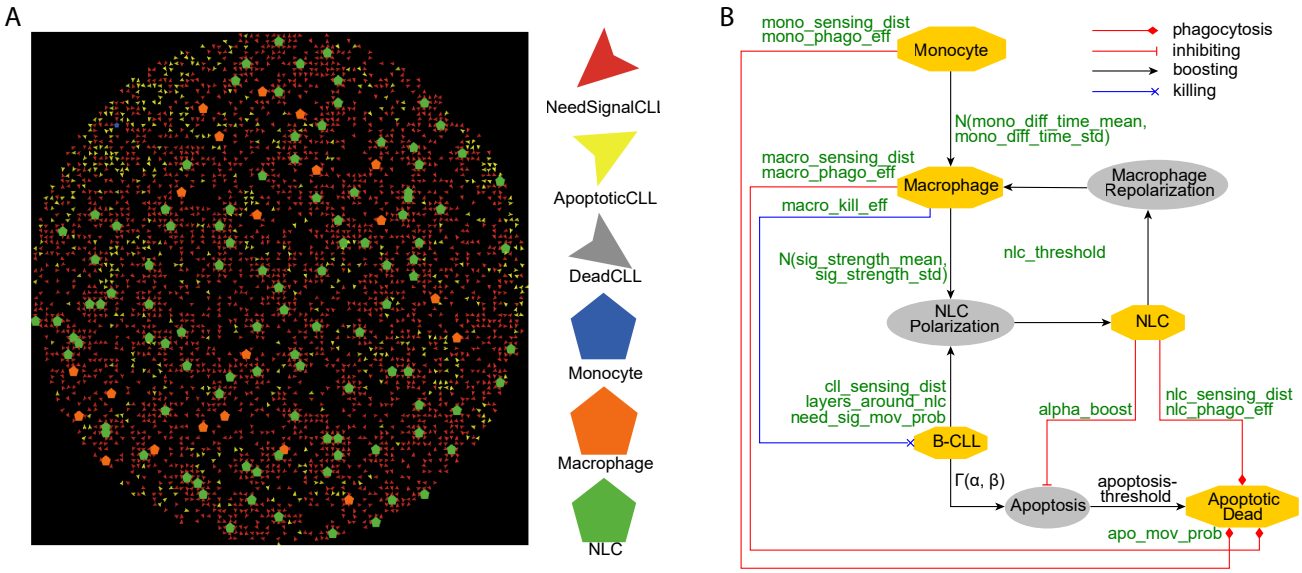

Fig. 2. Agent-based model representations. A) Simulation of 5000 cells in Netlogo. Cancer cells are depicted as small arrows (red, yellow or grey for need-signal, apoptotic or dead state, respectively) and myeloid cells are depicted as pentagons (blue, orange or green for monocytes, macrophages or NLCs, respectively). **B) Schematic diagram of the agent's behaviours.** Parameters calibrated based on experimental data are written in black and parameters optimized through the genetic algorithm are written in green. The arrows indicate the different cellular processes (phagocytosis/efferocytosis, killing) or the inhibiting/boosting roles on specific processes.

Parameter space exploration. Based on the two-dimensional ABM model of monocyte-to-NLC differentiation in presence of cancer B-CLL cells described in the previous section, we performed multiple simulations using various model parameters fixed to biologically reasonable values, allowing us to estimate the ranges to be systematically explored for each parameter (Supplementary Table S1). To determine the parameter values

able to reproduce the B-CLL survival dynamics observed experimentally in the PBMC autologous cultures, we then performed an optimization analysis employing the nondominated sorting genetic algorithm-II (NSGA-II, (42, 43), Fig. 3A), implemented in openMOLE (41). This procedure systematically generates populations of parameter sets and evolves the candidate solutions towards higher values of two objective fitness functions, corresponding to the fit between experimental data and model predictions on both B-CLL viability and concentration dynamics. We next calculated the Pareto front to identify the sets of parameters which represent the best trade-offs between the two objective constraints (Fig. 3B).

A total of 165 parameter sets were obtained as optimal solutions from the Pareto front, whose convex shape indicates the anti-correlated nature of the two fitnesses, as generally observed in bi-objective optimization (Fig. 3B). In addition, the distribution of each parameter value within solutions on the Pareto front (Fig. 4A) allows us to check for consistency between the result of the optimization algorithm and our biological observations. For example, monocyte phagocytosis efficiency is skewed towards low values, and macrophage phagocytosis efficiency towards high values, consistent with the biological observation that phagocytosis from non-adherent monocytes in the first days is negligible. Furthermore, higher values of alpha-boost are selected, representing the importance of the protective role of NLCs for B-CLL cells. To analyze the coupling between parameters, we further calculated their Pearson correlations and observed strong correlations amongst some of them. However, we decided not to combine the collinear parameters in order to preserve the biological processes that they represent explicitly in the model (Fig. 4B). Additionally, the Pearson correlations were also calculated between the parameters and the two fitness functions, suggesting a strong role for phagocytosis (especially NLC phagocytosis efficiency) in obtaining a higher viability fitness (Fig. 4C).

Model validation. Generally, in multi-objective optimization methods, choosing a specific set of parameters from the optimization results requires both biological and computational reasoning. In our case, we focused particularly on three parameter sets corresponding to (1) best fitness on viability (Fig. 3C), (2) best fitness on concentration and (3) knee point on the Pareto front, which is defined as the point on the Pareto front which is closest to the point that optimizes both constraints (Supplementary Fig. S2). Interestingly, we observed that model simulations with the three sets give considerably different system dynamics (Supplementary Fig. S2A-B). More specifically, the model defined with the parameters set

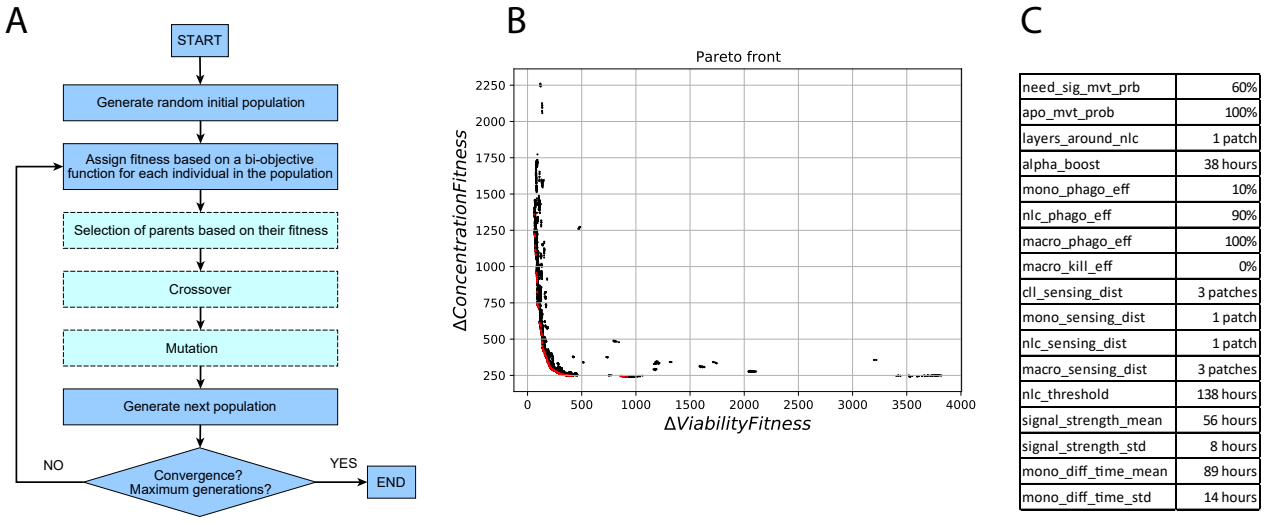

need_sig_mvt_prb	60%
apo_mvt_prob	100%
layers_around_nlc	1 patch
alpha_boost	38 hours
mono_phago_eff	10%
nlc_phago_eff	90%
macro_phago_eff	100%
macro_kill_eff	0%
cll_sensing_dist	3 patches
mono_sensing_dist	1 patch
nlc_sensing_dist	1 patch
macro_sensing_dist	3 patches
nlc_threshold	138 hours
signal_strength_mean	56 hours
signal_strength_std	8 hours
mono_diff_time_mean	89 hours
mono_diff_time_std	14 hours

Fig. 3. Overview of strategy and results of the parameter exploration. A) Schematic diagram of the bi-objective genetic algorithm. Flow chart of the NSGA-II algorithm procedure. The algorithm parameters are given in Supplementary Table S2. **B) Pareto front of the bi-objective search.** The NSGA-II genetic algorithm evaluates each explored set of parameters (20'000 generations) according to 2 objective functions corresponding to B-CLL viability and concentration, throughout each simulation (10 time points, least squares method). The Pareto front depicted in red here contains 165 non-dominated solutions. **C) Optimized parameters.** The parameters listed here were obtained from the parameters set maximizing the viability fitness.

matching the best fitness for viability produces two minima in viability and reaches a steady state in both viability and concentration, as observed experimentally after 13 days of culture (Fig. 1C). The set matching best fitness for concentration does not reproduce this dynamics and more importantly confers 0% of phagocytosis efficiency to the NLC class (Supplementary Fig. S2C), which is in contradiction with published data on NLCs. Finally, the set from the knee point does not generate the second viability minima that should occur around Day 10. For these reasons, we decided to focus on the parameter set which optimizes viability (Fig. 3C, Supplementary Table S1).

Using the parameters that maximize fitness on viability obtained from the exploration procedure, we observed a good fit between the simulation results and experimental data from B-CLL survival in PBMC autologous cultures averaged from 3 different patients (Fig. 5A). The opposing constraints between optimizing viability and concentration might prevent the algorithm from converging towards best fitting solutions on each objective independently, which could explain the few discrepancies between model prediction and experimental data. Satisfied by the ability of our model to reproduce experimental results, we turned to testing its predictive power. One of the main controlled parameters in the model is the initial concentration of monocytes in the culture. We therefore tested the predictive power of the model by varying the initial concentration of monocytes and estimating the B-CLL survival and concentration. We then compared our predictions to experiments from heterologous co-cultures of healthy monocytes with patient

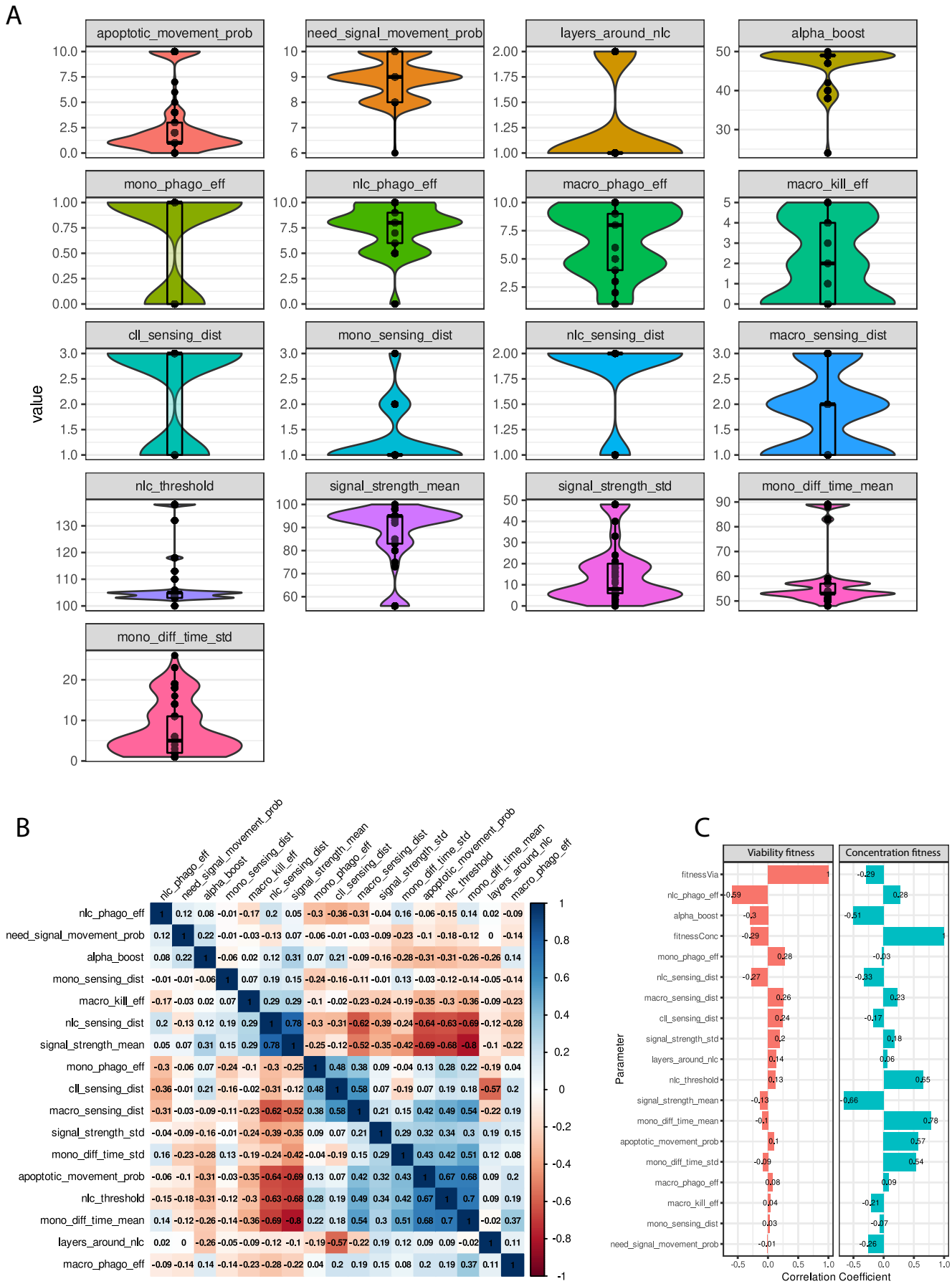

Fig. 4. Parameter distributions and correlations. A) Parameter distribution of the Pareto front solutions. The violin plots show the distribution of parameter values in the 165 non-dominated solutions of the Pareto front. **B) Pearson correlation coefficients between model parameters.** A hierarchical clustering with a complete method was applied to cluster the parameters. textbfC) Parameters' correlations with fitnesses. The parameters are ranked based on the absolute value of their correlation coefficient with viability fitness.

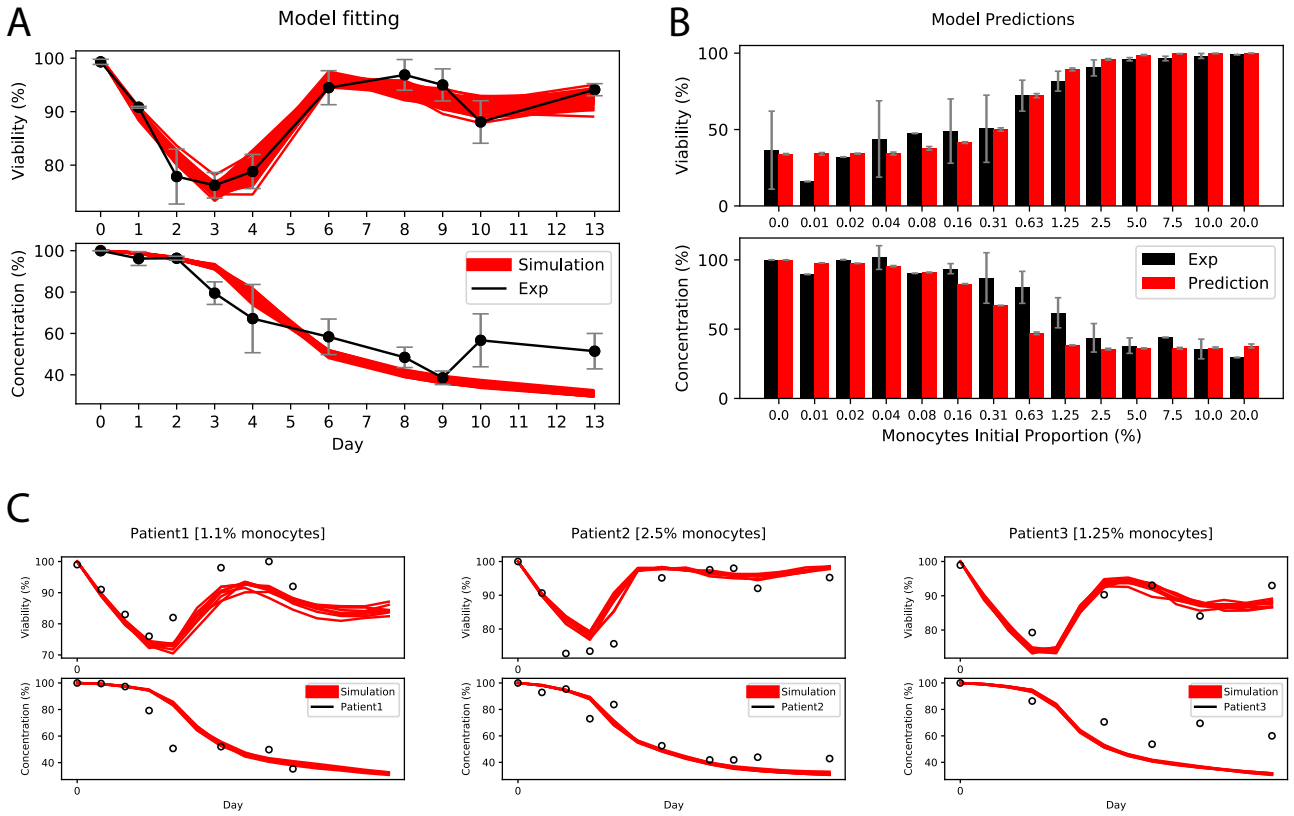

Fig. 5. Comparison of simulated and experimental time courses. A) Model fitting to experimental data. 100 simulations were run with the best set of parameters and compared with the averaged viability and concentration observed experimentally. The initial monocytes proportion for the simulations was set to 1.6% corresponding to the average monocytes proportion measured in the patients. Simulations are depicted in red and experimental data in black. **B) Predictions on heterologous co-cultures.** Simulations were run for varying initial monocytes proportions (3 repetitions) for 9 days and compared to experimental observations. Red bars correspond to the simulations and black bars correspond to the experimental data. **C) Patient-specific predictions.** 8 simulations were run with the best set of parameters and compared with the averaged viability and concentration observed experimentally. The initial monocytes proportion for the simulations was set to the specific percentage of monocytes measured in each patient (1.1%, 2.5% and 1.25%). Simulations are depicted in red and experimental data for the corresponding patient in black.

CLL cells in which we could vary initial monocyte concentration at will (Fig. 1D).

The results depicted in Fig. 5B show that the model is able to predict viability and concentration values observed experimentally with changing initial monocyte concentration. The initial monocyte concentration could be a factor that partially explains the broad differences in experimental data from different patients. We therefore tested whether we could make patient-specific simulations using our general model by tuning the initial monocyte concentration to the patient-specific measured values of this parameter. In this context, our predictions of B-CLL viability and concentration also matched the experimentally observed profiles (Fig. 5C). These results suggest that the model could potentially be used to predict the patient's characteristics in terms of NLC production and even resistance to treatment, considering that NLCs are known to promote B-CLL survival and confer resistance to chemotherapy.

Parameter sensitivity analysis suggests a fundamental role for phagocytosis. To better understand the influence of specific parameters on the overall B-CLL survival dynamics, we performed a systematic sensitivity analysis varying each parameter while leaving the others at their optimized value (Fig. 6). We first explored the importance of phagocytosis by performing simulations varying the characteristic phagocytosis efficiencies of monocytes, macrophages and NLCs, highlighting an important impact of these parameters on the B-CLL viability dynamics (Fig. 7). We also show that models that do not have any phagocytosis cannot reproduce the experimentally observed dynamics and cannot predict the impact of varying initial monocyte concentrations (Fig. 6A-C), even with higher values of NLC protection (*alpha_boost*, Supplementary Fig. S4). We further explored the importance of the NLC protective effect on cancer cells by running simulations with varying values of the corresponding protective chemical (*alpha_boost*, Fig. 6I). We observed that its role is particularly impactful towards the end of the culture, when NLCs already formed, and a high value of *alpha-boost* is necessary for a second increase in viability around day 10, as seen in the experiment. Next, we evaluated the importance of the threshold that determines after how long a macrophage turns into NLC, finding that it also strongly impacts the viability dynamics (Fig. 6D-E). The differentiation time of monocytes into macrophages was also shown to influence the survival dynamics as displayed by the simulations using varying parameters at initialization (Fig. 6F). Interestingly, the presence of two distinct minima in viability (around day 3 and day 10) depends on the relative macrophages and NLCs sensing distances (Fig. 6G-H). These correspond to the distances from which these cells are able to detect apoptotic and dead B-CLL to phagocyte them. Only a configuration in which macrophages can sense and phagocyte B-CLL from a higher distance than NLCs gives rise to a second viability minimum at day 10. On the contrary, B-CLL movement probabilities and macrophage killing efficiency were shown not to have a considerable impact on B-CLL survival dynamics with this set of optimized parameters (Supplementary Material, Fig. S3).

Discussion

The presence of TAMs in solid tumors hinders the efficacy of immunotherapy, which can be extremely beneficial in a subset of patients. Given the difficulty of studying cellular dynamics in tissues, we turned to an *in-vitro* model of leukemia, in which we can closely follow the production of TAMs from monocytes in the presence of cancer cells. Building on experimental measurements of cell counts and viability of cancer

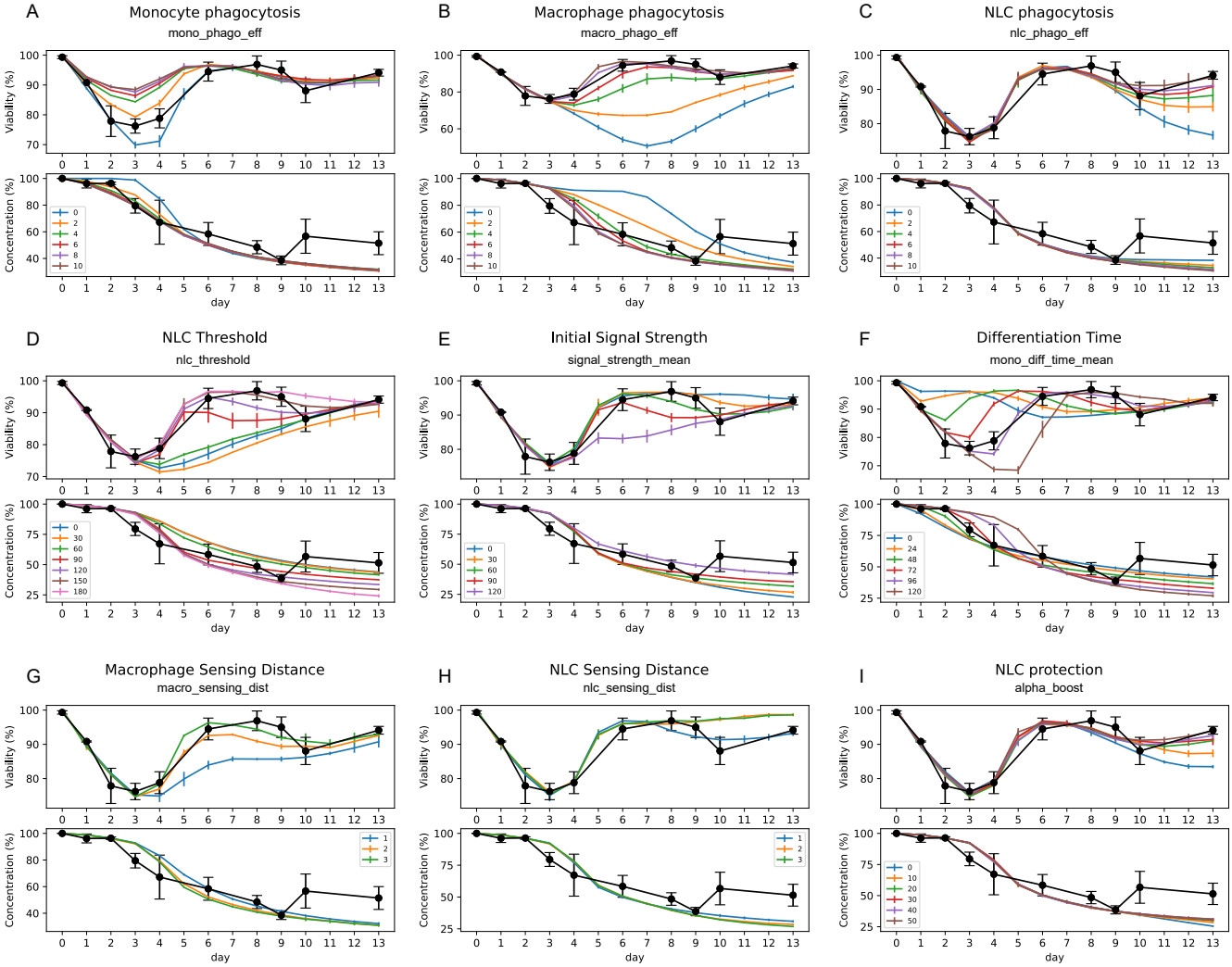

Fig. 6. Parameter sensitivity analysis. The parameters were varied one at a time while keeping all other parameters constant to estimate their impact on the overall dynamics. Parameters which were the most impactful are displayed here. Figures related to the other parameters can be found in Supplementary Fig. S3.

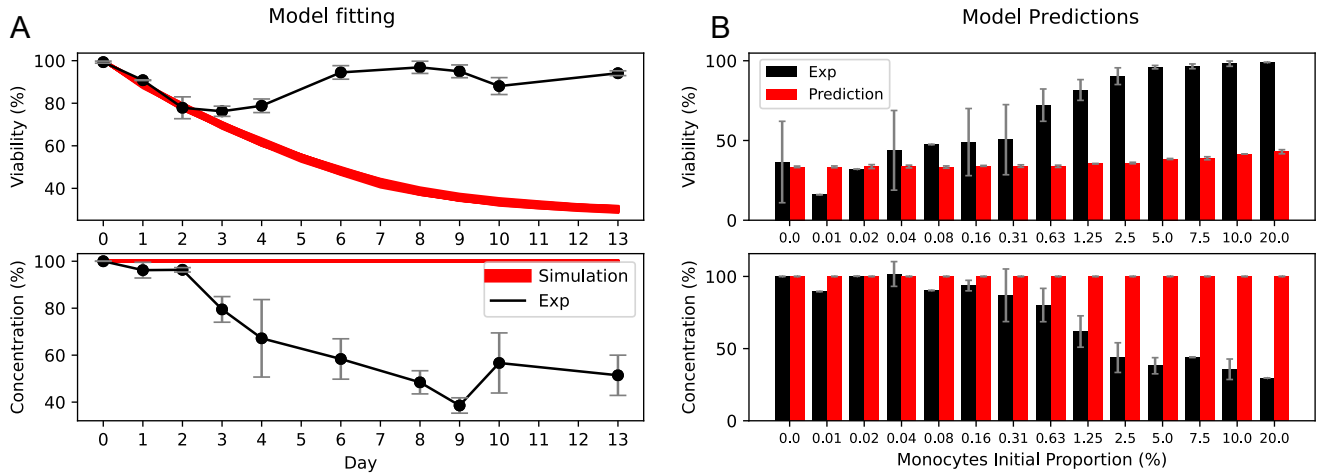

Fig. 7. Impact of absence of phagocytosis on the model. Model simulations A) and prediction B) in absence of phagocytosis from monocytes, macrophages and NLCs.

cells in cultures of blood from Chronic Lymphocytic Leukemia patients, we implemented a two-dimensional agent-based model to simulate intercellular interactions in the spatial context of an *in-vitro* culture. More specifically, we modelled the interaction between cancer cells and monocytes, and the resulting differentiation of monocytes into macrophages that protect cancer cells (Nurse-Like Cells in this pathology). Using our experimental observations of cell viability and concentration in a time course to optimize the model parameters, we reproduced biologically realistic dynamics. We further tested the model's predictive power by simulating specific quantitative dynamics of NLC production in relation to the initial proportion of monocytes in co-cultures of healthy monocytes with CLL cells. These observations suggest that our models could be made patient-specific using this routinely measured variable. Finally, we analyzed the impact of the different parameters and suggest a strong role for phagocytosis in monocytes and NLCs to ensure the survival of cancer cells in this *in-vitro* CLL model, especially in the initial phases of the time course. The protective anti-apoptotic signals that are known to be provided by NLCs to the cancer cells (18) appear to be important especially towards the later stages of the culture. This finding suggests that monitoring and potentially modulating phagocytosis could play a role in the control of Tumor-Associated-Macrophage formation even in solid tumors. One possible reason for the importance of phagocytosis in this system lies in the need for cancer cells to establish physical contact with the NLC to benefit from their protective signals. A denser and more crowded environment with static dead cells would hinder the movement of living cancer cells toward the NLCs. Experimental validation will be necessary to investigate this hypothesis further. A discrepancy is often observed between our predicted concentration and experimental values at

the very end of the culture, with our simulations predicting lower concentrations. We could tentatively speculate that this could be explained by a low level of proliferation in the culture, which was not expected and not simulated due to lack of biological evidence, but which could improve the accuracy of our model (Supplementary Figure S5). Further work will be devoted to exploring this possibility.

There are some important limitations of this study that we will list below. As far as the experiments are concerned, these *in-vitro* cultures might not fully represent what is happening in the patient lymph nodes, where the density of CLL cells is as high as what we reproduce in the cultures, but potentially different cell populations other than cancer cells and monocyte/macrophages can be present in different proportions and within a different physical environment. For example, in our cultures, monocytes differentiate into macrophages in contact with the culture plate, something which is clearly artificial. Moreover, to be able to explore the impact of initial monocyte concentrations and thus validate the predictive power of our model, heterologous cultures of healthy monocyte donors and patient CLL cells were used. On one side, the interactions between cells from different individuals could introduce a cross-reactive immunity, and on the other side we might be introducing effects due to the specific (epi)genetic characteristics of the healthy donors.

Heterogeneity across patients is well known and the production of NLCs is extremely patient-specific in both time scales and number of NLCs produced. We are aware that different dynamics could be at play in different patients, and we hope that clinically measurable parameters, such as the initial monocyte concentration in the blood and others, could help us produce a generally useful model that can give specific predictions. However, this involves making strong assumptions about the fact that the same processes are active in different patients, which remains to be verified.

Regarding the ABM, we decided to model the system in two dimensions, since the macrophages are adherent to the plate and most of the dynamics is determined by what happens on this surface. One of the main advantages of ABMs against other types of models is the ease with which spatial information can be integrated. We therefore plan to expand our experiment to be able to capture spatial patterns in the culture that can be easily compared to those appearing in our simulations. The initialization of these simulations is currently stochastic and does not take into account any information that could be extracted from high content imaging of the cultures. Despite this interesting prospect, the high density of cancer cells

in the cultures have made quantitative imaging particularly difficult and we will explore these possibilities in further work.

An obvious extension of this model would involve simulating cellular dynamics in tissues, thus tackling the issue of TAM formation in solid tumors. We have recently developed tools to extract spatial information from tumor tissue samples either imaged via microscopy or characterized through single-cell spatial-omics techniques (44), and we plan to establish a framework to use spatial data to initialize the ABM simulations in these more complex contexts.

Finally, we realize the importance of internal regulatory processes that determine the agents' behaviors and plan to extend this model by combining it with gene regulatory network models of phenotype transitions inside each cell (cancer cells, monocytes and potentially other cells present in the TME of solid tumors in considerable proportions such as lymphocytes or fibroblasts). More specifically, we have been working on a Boolean model of monocyte differentiation into NLCs that we plan to integrate to the presented ABM model using suitable tools in further work (16, 37, 38).

To conclude, we hope that this model can be a starting point to provide mechanistic simulations of dynamic cellular interactions in the tumor microenvironment, able to take into account patient-specific characteristics, and useful to generate novel biological hypotheses.

Materials and Methods

Cell culture. Blood samples were obtained after informed consent and stored at the HIMIP collection. According to French law, the HIMIP collection was declared to the Ministry of Higher Education and Research (DC 2008-307 collection 1) and a transfer agreement (AC 2008-129) was agreed after approbation by the "Comité de Protection des Personnes Sud-Ouest et Outremer II" (ethical committee). Clinical and biological annotation of samples were declared to the Comité National Informatique et Libertés (CNIL; data processing and liberties national committee). PBMCs were isolated from the blood of CLL patients or buffy-coat from the healthy donors (HD). To generate autologous NLC, PBMC from CLL patient were cultured at 10^7 cells/mL in RPMI 1640 supplemented with 10% Fetal Calf Serum and and 1% Penicillin/Streptomycin (Gibco) in the incubator at 37 °C with 5% CO2. Cells were cultured for 13 days during which differentiation of the NLC was followed by BFI microscopy and phenotype of the cells was assessed by flow cytometry (presence of CD14, CD163 and CD206) at the final day of the culture. At the indicated time points B-CLL cells samples were taken to measure cell concentration by hemocytometer and cell viability by flow cytometry using AnnexinV/7-AAD staining. To generate heterologous co-culture, B-CLL from PBMC fraction were

isolated using negative selection (EasySep™ Human B Cell Enrichment Kit II Without CD43 Depletion, STEMcell) and monocytes from HD PBMC were isolated using positive selection method(CD14 MicroBeads, human, Miltneyi). Subsequently B-CLL cells at 107 c/mL were mixed with varying concentrations of purified monocytes. At day 9 concentration and viability of the B-CLL cells was measured and the phenotype of NLC was assessed by FACS. CLL PBMC used for the experiment contained >85% of B-CLL cells and 0,5-2% of monocytes as assessed by flow cytometry. Purity of the isolated B-CLL and monocytes exceeded 95%.

Agent Based Model. The ABM was implemented in NetLogo (39, 40), mimicking a projection of a cylindrical plate. In general, macrophages and NLCs perform most of their functions after adherence, therefore the model was built in 2D. The simulation duration was set to 13 days with each simulation time step corresponding to 1 hour. At each time step, the following processes are executed by each cell in the following order:

- **update-position**: movements are either random or directional (e.g. the cancer cells move towards *NLCs*, and the *macrophages/NLCs* move towards *apoptotic* or *dead* cancer cells). Movements concern all cells except the dead ones, which are immobile.
- **update-phagocytosis**: this concerns the movement of a myeloid cell onto a cancer cell within a characteristic perception radius (or *sensing_distance*). If the myeloid cell encounters a *dead* or *apoptotic* cancer cell, it will phagocyte it with characteristic efficiencies (*phagocytosis_efficiency*), and the phagocytosed cancer cell is removed from the simulation. If the myeloid cell does not find a cell to phagocyte within its perception radius, it will move randomly to a surrounding patch. Additionally, macrophages are able to phagocyte living B-CLL cells in the need-signal state with a specific killing-efficiency.
- **update-properties**: increases or decreases *life* value for cancer cells (+1, -1, +*alpha_boost*), *signal_strength* for myeloid cells (+1, -1), or the amount of anti-apoptotic signals (referred to as chemical-A) on patches (+1, -1, diffusion).
- **update-class**: based on their properties values and specific calibrated thresholds, cells might change their state (class) at the next time step. For example, an *apoptotic* cancer cell will convert to dead if its life value goes below a certain threshold (*death_threshold*), need-signal cancer cells will turn into *apoptotic* cells if their *life* goes below *apoptosis_threshold*. Myeloid cells will differentiate from monocyte to macrophage depending on their differentiation timing, and polarize from macrophage to NLC or from NLC to macrophage, depending on their *signal_strength* compared to *nlc_threshold*.

For each cell state (class), the following actions are considered:

- ***Monocytes*** can perform 3 actions: move, differentiate into *macrophages* and perform phagocytosis. At the start of the simulation, *monocytes* start to adhere and differentiate into macrophages in a time window spanning

from 60h to 96h (*mono_diff_time_mean*). Variability in this process is also explored (*mono_diff_time_std*). *Monocytes* can move towards *apoptotic* or *dead* B-CLL cells in their perception radius (*mono_sensing_dist*), and will phagocyte these cells with their characteristic efficiency (*mono_phago_eff*).

- ***Macrophages*** can perform 4 actions: move, phagocytosis, polarization and killing the living (*need-signal*) cancer cells. Similarly to *monocytes*, they can move towards *apoptotic* or *dead* cells in their perception radius (*macro_sensing_dist*) and phagocyte them with their characteristic efficiency (*macro_phago_eff*), whereas the killing of living B-CLL cells (*need-signal*) is performed with another characteristic efficiency (*macro_kill_eff*). At each time step, the number of contacts between macrophages and B-CLL cells (*need-signal* and *apoptotic*) is counted and the polarization into *NLC* occurs when the *macrophages* have been in contact with B-CLL cells a sufficient duration (*nlc_threshold*). The polarization process is reversible.

- ***NLCs*** can perform 4 actions: move, phagocytosis of *apoptotic* or *dead* B-CLL cells, secretion of anti-apoptotic signals (chemical-A) on patches and re-polarization into *macrophages*. Similar to *macrophages*, *NLCs* will move in the direction of *apoptotic* and *dead* CLL cells in their perception radius (*nlc_sensing_dist*) and will phagocyte them with their characteristic efficiency (*nlc_phago_eff*). If the *NLCs* are not surrounded anymore by a sufficient amount of (*need-signal*) cancer cells, their *signal_strength* will decrease and they will eventually re-polarize into *macrophages* if it goes below *nlc_threshold*.

- **B-CLL cancer cells** can be in 3 states (*need-signal*, *apoptotic* or *dead*), each of which will influence the cancer cell's behavior. In the ***need-signal*** state, B-CLL cells search for *NLCs* around them in a characteristic perception radius (*cll_sensing_dist*) and will move towards that direction, or randomly in the absence of surrounding *NLCs*. When B-CLL cancer cells find *NLCs* they will remain attached to them on n layers (with n being the number of layers of B-CLL that NLC can have around them, i.e. *layers_around_nlc*). Importantly, when B-CLL cancer cells move on patches containing anti-apoptotic signals (chemical-A), they consume a part of it, and get an increment of *alpha_boost* on their *life* property value, which helps them fight apoptosis and survive longer. In the ***apoptotic*** state, the cancer cells can no longer benefit from the anti-apoptotic signals from *NLCs* and will subsequently die. They can be phagocytosed. In the ***dead*** state, cells can no longer move and can also be phagocytosed.

States and counters are updated at each time step. *nlc-threshold* is a proxy for the number of accumulated hours for which a *macrophage* has been in contact with at least one *need-signal* or *apoptotic* cancer cell. In the model, *need-signal* and *apoptotic* cells move with a calibrated probability (from 0% to 100%) whereas *dead* cells do not move at all.

Code availability. All the files used for model simulation in Netlogo, parameter optimization in OpenMOLE and statistical analysis of the outputs are available in Github.

1. Manpreet Sambi, Leila Bagheri, and Myron R Szewczuk. Current challenges in cancer immunotherapy: multimodal approaches to improve efficacy and patient response rates. *Journal of oncology*, 2019, 2019.
2. Alessandro Palma, Abdul Salam Jarrah, Paolo Tieri, Gianni Cesareni, and Filippo Castiglione. Gene regulatory network modeling of macrophage differentiation corroborates the continuum hypothesis of polarization states. *Frontiers in physiology*, 9:1659, 2018.
3. Fernando O Martinez and Siamon Gordon. The m1 and m2 paradigm of macrophage activation: time for reassessment. *F1000prime reports*, 6, 2014.
4. Shweta Aras and M Raza Zaidi. Tameless traitors: macrophages in cancer progression and metastasis. *British journal of cancer*, 117(11):1583–1591, 2017.
5. Roy Noy and Jeffrey W Pollard. Tumor-associated macrophages: from mechanisms to therapy. *Immunity*, 41(1):49–61, 2014.
6. Alberto Mantovani, Paola Allavena, and Antonio Sica. Tumour-associated macrophages as a prototypic type ii polarised phagocyte population: role in tumour progression. *European journal of cancer*, 40(11):1660–1667, 2004.
7. L. Bingle, N. J. Brown, and C. E. Lewis. The role of tumour-associated macrophages in tumour progression: Implications for new anticancer therapies. *Journal of Pathology*, 196(3):254–265, 2002. .
8. Luca Cassetta and Jeffrey W Pollard. Targeting macrophages: Therapeutic approaches in cancer, Nov 2018. ISSN 14741784. URL https://www.nature.com/articles/nrd.2018.169.
9. Maurilio Ponzoni, Claudio Doglioni, and Federico Caligaris-Cappio. Chronic lymphocytic leukemia: the pathologist's view of lymph node microenvironment. In *Seminars in diagnostic pathology*, volume 28, pages 161–166. Elsevier, 2011.
10. Jan A Burger. Nurture versus nature: the microenvironment in chronic lymphocytic leukemia. *Hematology 2010, the American Society of Hematology Education Program Book*, 2011(1):96–103, 2011.
11. Rachel E Hayden, Guy Pratt, Claudia Roberts, Mark T Drayson, and Chris M Bunce. Treatment of chronic lymphocytic leukemia requires targeting of the protective lymph node environment with novel therapeutic approaches. *Leukemia & lymphoma*, 53(4):537–549, 2012.
12. Yair Herishanu, Patricia Pérez-Galán, Delong Liu, Angélique Biancotto, Stefania Pittaluga, Berengere Vire, Federica Gibellini, Ndegwa Njuguna, Elinor Lee, Lawrence Stennett, et al. The lymph node microenvironment promotes b-cell receptor signaling, nf-κb activation, and tumor proliferation in chronic lymphocytic leukemia. *Blood, The Journal of the American Society of Hematology*, 117(2): 563–574, 2011.
13. Agata A Filip, Bogumiła Ciseł, and Ewa Wąsik-Szczepanek. Guilty bystanders: nurse-like cells as a model of microenvironmental support for leukemic lymphocytes. *Clinical and experimental medicine*, 15(1):73–83, 2015.
14. F Boissard, JJ Fournie, A Quillet-Mary, L Ysebaert, and M Poupot. Nurse-like cells mediate ibrutinib resistance in chronic lymphocytic leukemia patients. *Blood cancer journal*, 5(10):e355–e355, 2015.
15. Elisa Ten Hacken and Jan A Burger. Microenvironment interactions and b-cell receptor signaling in chronic lymphocytic leukemia: Implications for disease pathogenesis and treatment. *Biochimica et Biophysica Acta (BBA)-Molecular Cell Research*, 1863(3):401–413, 2016.
16. Malvina Marku, Nina Verstraete, Flavien Raynal, Miguel Madrid-Mencía, Marcin Domagala, Jean-Jacques Fournié, Loïc Ysebaert, Mary Poupot, and Vera Pancaldi. Insights on tam formation from a boolean model of macrophage polarization based on in vitro studies. *Cancers*, 12(12):3664, 2020.
17. Li Jia, Andrew Clear, Feng-Ting Liu, Janet Matthews, Nadiha Uddin, Aine McCarthy, Elena Hoxha, Catherine Durance, Sameena Iqbal, and John G Gribben. Extracellular hmgb1 promotes differentiation of nurse-like cells in chronic lymphocytic leukemia. *Blood, The Journal of the American Society of Hematology*, 123(11):1709–1719, 2014.
18. F Boissard, C Laurent, AG Ramsay, A Quillet-Mary, JJ Fournie, M Poupot, and L Ysebaert. Nurse-like cells impact on disease progression in chronic lymphocytic leukemia. *Blood cancer journal*, 6(1): e381–e381, 2016.
19. Jan A Burger, Meike Burger, and Thomas J Kipps. Chronic lymphocytic leukemia b cells express functional cxcr4 chemokine receptors that mediate spontaneous migration beneath bone marrow stromal cells. *Blood, The Journal of the American Society of Hematology*, 94(11):3658–3667, 1999.
20. Jan A Burger and Thomas J Kipps. Chemokine receptors and stromal cells in the homing and homeostasis of chronic lymphocytic leukemia b cells. *Leukemia & lymphoma*, 43(3):461–466, 2002.
21. Hugo Talbot, Sofiane Saada, Elodie Barthout, Paul-François Gallet, Nathalie Gachard, Julie Abraham, Arnaud Jaccard, Danielle Troutaud, Fabrice Lalloué, Thomas Naves, et al. Bdnf belongs to the nurse-like cell secretome and supports survival of b chronic lymphocytic leukemia cells. *Scientific reports*, 10(1):1–9, 2020.
22. Mitsufumi Nishio, Tomoyuki Endo, Nobuhiro Tsukada, Junko Ohata, Shinichi Kitada, John C Reed, Nathan J Zvaifler, and Thomas J Kipps. Nurselike cells express baff and april, which can promote survival of chronic lymphocytic leukemia cells via a paracrine pathway distinct from that of sdf-1α. *Blood*, 106(3):1012–1020, 2005.
23. Charles M Macal and Michael J North. Agent-based modeling and simulation. In *Proceedings of the 2009 Winter Simulation Conference (WSC)*, pages 86–98. IEEE, 2009.
24. Gary An, Qi Mi, Joyeeta Dutta-Moscato, and Yoram Vodovotz. Agent-based models in translational systems biology. *Wiley Interdisciplinary Reviews: Systems Biology and Medicine*, 1(2):159–171, 2009.
25. Angela Reynolds, Jonathan Rubin, Gilles Clermont, Judy Day, Yoram Vodovotz, and G Bard Ermentrout. A reduced mathematical model of the acute inflammatory response: I. derivation of model and analysis of anti-inflammation. *Journal of theoretical biology*, 242(1):220–236, 2006.
26. Alva Presbitero, Emiliano Mancini, Ruud Brands, Valeria V Krzhizhanovskaya, and Peter Sloot. Supplemented alkaline phosphatase supports the immune response in patients undergoing cardiac surgery: clinical and computational evidence. *Frontiers in immunology*, 9:2342, 2018.

27. Zarifeh Heidary, Jafar Ghaisari, Shiva Moein, and Shaghayegh Haghjooy Javanmard. The double-edged sword role of fibroblasts in the interaction with cancer cells; an agent-based modeling approach. *PloS one*, 15(5):e0232965, 2020.

28. Zhihui Wang, Joseph D Butner, Romica Kerketta, Vittorio Cristini, and Thomas S Deisboeck. Simulating cancer growth with multiscale agent-based modeling. In *Seminars in cancer biology*, volume 30, pages 70–78. Elsevier, 2015.

29. Erin N Bodine, Robert M Panoff, Eberhard O Voit, and Anton E Weisstein. Agent-based modeling and simulation in mathematics and biology education. *Bulletin of Mathematical Biology*, 82(8):1–19, 2020.

30. Dimitrios Voukantsis, Kenneth Kahn, Martin Hadley, Rowan Wilson, and Francesca M Buffa. Modeling genotypes in their microenvironment to predict single-and multi-cellular behavior. *GigaScience*, 8 (3):giz010, 2019.

31. Boris Aguilar, David L Gibbs, David J Reiss, Mark McConnell, Samuel A Danziger, Andrew Dervan, Matthew Trotter, Douglas Bassett, Robert Hershberg, Alexander V Ratushny, et al. A generalizable data-driven multicellular model of pancreatic ductal adenocarcinoma. *GigaScience*, 9(7):giaa075, 2020.

32. Angela Schulz, Claudia Dürr, Thorsten Zenz, Hartmut Döhner, Stephan Stilgenbauer, Peter Lichter, and Martina Seiffert. Lenalidomide reduces survival of chronic lymphocytic leukemia cells in primary cocultures by altering the myeloid microenvironment. *Blood, The Journal of the American Society of Hematology*, 121(13):2503–2511, 2013.

33. Kerri-Ann Norton, Travis Wallace, Niranjan B Pandey, and Aleksander S Popel. An agent-based model of triple-negative breast cancer: the interplay between chemokine receptor ccr5 expression, cancer stem cells, and hypoxia. *BMC systems biology*, 11(1):1–15, 2017.

34. Kerri-Ann Norton, Chang Gong, Samira Jamalian, and Aleksander S Popel. Multiscale agent-based and hybrid modeling of the tumor immune microenvironment. *Processes*, 7(1):37, 2019.

35. Gianluca D'Antonio, Paul Macklin, and Luigi Preziosi. An agent-based model for elasto-plastic mechanical interactions between cells, basement membrane and extracellular matrix. *Mathematical biosciences and engineering: MBE*, 10(1):75, 2013.

36. Yafei Wang, Heber Rocha, Randy Heiland, and Paul Macklin. Simulation of drug-loaded nanoparticles on cancer treatment: an agent-based modelling approach. In *2021 Joint Mathematics Meetings (JMM)*. AMS, 2021.

37. Ahmadreza Ghaffarizadeh, Randy Heiland, Samuel H Friedman, Shannon M Mumenthaler, and Paul Macklin. Physicell: An open source physics-based cell simulator for 3-d multicellular systems. *PLoS computational biology*, 14(2):e1005991, 2018.

38. Gaelle Letort, Arnau Montagud, Gautier Stoll, Randy Heiland, Emmanuel Barillot, Paul Macklin, Andrei Zinovyev, and Laurence Calzone. Physiboss: a multi-scale agent-based modelling framework integrating physical dimension and cell signalling. *Bioinformatics*, 35(7):1188–1196, 2019.

39. Elizabeth Sklar. Netlogo, a multi-agent simulation environment. *Artificial life*, 13(3):303–311, 2007.

40. Seth Tisue and Uri Wilensky. Netlogo: A simple environment for modeling complexity. In *International conference on complex systems*, volume 21, pages 16–21. Boston, MA, 2004.

41. Romain Reuillon, Mathieu Leclaire, and Sebastien Rey-Coyrehourcq. Openmole, a workflow engine specifically tailored for the distributed exploration of simulation models. *Future Generation Computer Systems*, 29(8):1981–1990, 2013.

42. Kalyanmoy Deb. Evolutionary algorithms. In *Multi-objective optimization using evolutionary algorithms*, pages 81–170. John Wiley & Sons, Ltd, 2001.

43. Kalyanmoy Deb, Amrit Pratap, Sameer Agarwal, and TAMT Meyarivan. A fast and elitist multiobjective genetic algorithm: Nsga-ii. *IEEE transactions on evolutionary computation*, 6(2):182–197, 2002.

44. Alexis Coullomb and Vera Pancaldi. Tysserand—fast and accurate reconstruction of spatial networks from bioimages. *Bioinformatics*, 37(21):3989–3991, 2021.